Monografías del Seminario Matemático García de Galdeano **33**, 369–376 (2006)

FLUID-STRUCTURE COUPLING OF A TURBULENT FLOW AND A GENERIC BLIMP STRUCTURE AT HIGH ANGLE OF ATTACK

K. El Omari, E. Schall, B. Koobus,
A. Dervieux, M. Amara and J.-P. Dumas

Abstract. We present here a numerical study of the aeroelastic behavior of a pressurized flexible airship (blimp) during a flight with an angle of attack of 20°. The airship is represented by a 6:1 prolate spheroid generic geometry . The air flow is fully turbulent and is modeled by a LES model. We solve the Navier-Stokes three-dimensional compressible equations in their ALE form. The spatial discretization of these equations is achieved on unstructured tetrahedral meshes by a Finite Volumes/Finite Elements (FV/FE) mixed formulation. This fluid simulation is coupled to a structure solver by a staggered algorithm. We investigate a flexible pressurized hull compared to a non-pressurized one.

Keywords: Aeroelastic, turbulence, airship, finite volumes, finite elements, LES, ALE, GCL, MUSCL

§1. Introduction

High load airships got a regain of interest in the last decade. These airships are of large dimensions ($\sim 300\,m$ long) and are intended to carry up to 250 tons of freight. They are expected to be an economic transport way, using less ground infrastructures compared to traditional aeronautic vehicles and subject to less statutory restrictions (ex: noise regulations...). The development of these large airships is in its beginnings on the contrary to the moderated size ones, which were subject to more developments and exploitation, essentially for advertising purposes.

There are two main categories of airships by regard to their structures: rigid and elastic (blimps). Elastic structures are pressurized to make them sufficiently rigid. For large dimensions blimps, rigidity can be enhanced by additional stiffeners (semi-rigid airships).

During an airship flight, the air flow is characterized by a high Reynolds number due to the large airship dimensions, while the Mach number remains relatively low and the flow weakly compressible. This flow is fully turbulent and may generates large vortical features, especially at high angle of attack (ex: lateral wind). The structure of a flying airship is subject to substantial deformations, particularly if it is non-rigid and of large dimensions.

This work is a first step of a study of the aeroelastic behavior of a pressurized airship. Thus, the adopted geometry is a generic one, based on a $6:1$ prolate spheroid of $L = 1.37\,m$ length. This geometry has been the subject of several experimental [1] and numerical [2] studies concerning high Reynolds turbulent flows ($Re = 4.2 \times 10^6$).

We intend here to study the air flow at a lower Reynolds number coupled to the modeling of the deforming structure. This study in the continuation of a previous study that was concerned by a harder metallic hull [3].

§2. Numerical approach

2.1. The aeroelastic problem

The whole behavior of the deforming hull under the fluid action can be modeled by a three-field problem:

- Fluid: the Navier-Stokes turbulent equations on an Arbitrary Lagrangian Eulerian (ALE) formulation;
- Structure: classical elastodynamic equations;
- Mesh: a discrete pseudo-structural system.

The global equations of the problem can be written as:

$$\left.\frac{\partial (JW)}{\partial t}\right|_{\xi} + J\nabla_x \cdot (F(W) - \dot{x}W) = J\nabla_x \cdot R(W) + JS(W), \tag{1}$$

$$\rho_S \frac{\partial^2 u_S}{\partial t^2} - \nabla_{\mathscr{X}} \cdot \sigma_S(u_S) = b, \tag{2}$$

$$\tilde{\rho}\frac{\partial^2 X}{\partial t^2} - \nabla_x \cdot \tilde{\sigma}(X) = g(u_S), \tag{3}$$

with:

$x(t)$: position of fluid domain points,	ξ: position in a reference configuration,
W: fluid state vector,	$J = \det(\frac{\partial x}{\partial \xi})$, $\quad \dot{x} = \frac{\partial x}{\partial t}\|_{\xi}$,
u_S: displacement field of the structure,	F and R convective and diffusive ALE fluxes,
X: displacement field of the mesh,	σ_S: structure stress tensor,
$\tilde{\sigma}$: fictitious stress tensor,	$g(u_S)$: action of the motion of the structure.

These equations are coupled by their boundary conditions ensuring the continuity of velocities and forces between the fluid and the structure and the continuity of velocities and positions between the fluid mesh and the structure:

Fluid (W)/Structure (u_S):	Fluid mesh(X)/Structure (u_S):
$\sigma_S \cdot n = (-p + \sigma_F) \cdot n \quad$ and $\quad v_F = \dfrac{\partial u_S}{\partial t}$	$X = u_S \quad$ and $\quad \dfrac{\partial X}{\partial t} = \dfrac{\partial u_S}{\partial t} = v_F$

2.2. Spatial discretizations

2.2.1. ALE fluid solver

We solve the Navier-Stokes three-dimensional compressible equations. The spatial discretization of these equations is achieved on unstructured tetrahedral meshes by a mixed Finite

Volumes/Finite Elements (FV/FE) formulation [4], where the convective terms are discretized by a FV method and the diffusive terms are approximated by a Galerkin method using P1 shape functions.

The convective fluxes are approached by the Roe's scheme, which is extended by a MUSCL linear reconstruction method [4] to obtain a higher order of spatial accuracy. These fluxes are integrated over vertices centered dual cells as:

$$\int_{\partial C_i(t)} (F(W) - \dot{x}W).n\,d\sigma = \sum_{j \in V(i)} \Phi^{Roe}(W_i, W_j, n_{ij}, \sigma_{ij}) + \Phi^{SW}_{\Gamma_\infty}(W_i, W_\infty, n_{i\infty}, \sigma_{i\infty}),$$

where $\Phi^{SW}_{\Gamma_\infty}$ is the Steger and Warming flux at far-field boundaries. In the ALE form, the Roe's numerical flux is written:

$$\begin{aligned}\Phi^{Roe}(u,v,n,\sigma) = &\frac{1}{2}\left[F(u).n - \sigma|n|u + F(v).n - \sigma|n|v\right] \\ &- \gamma P^{-1}\left|P\left(\frac{\partial F}{\partial W}(\tilde{W},n) - \sigma|n|I_d\right)\right|\left(\frac{v-u}{2}\right),\end{aligned}$$

where appears the Roe-Turkel preconditioner P, useful for low Mach number flows. By the MUSCL extension, the Roe's numerical flux is rewritten in the form $\Phi^{Roe}(W_{ij}, W_{ji}, n_{ij}, \sigma_{ij})$, with:

$$W_{ij} = W_i + \frac{1}{2}(\nabla W)_i \cdot (x_j - x_i), \quad W_{ji} = W_j - \frac{1}{2}(\nabla W)_j \cdot (x_j - x_i).$$

Concerning the turbulent character of the flow, a Large Eddy Simulation (LES) is used with the Smagorinsky model. This code feature was widely used to solve flows with vortex shedding [5, 6]. This turbulent approach is coupled with weakly dissipative MUSCL formulation using a numerical viscosity that is based on a sixth order derivatives. This formulation reduces the interaction between the numerical dissipation and LES subgrid model [5].

The code is parallel and uses non-overlapping decomposition of the computational mesh.

2.2.2. Structure solver

The structure solver is based on a finite elements model that predicts the true displacements, velocities and accelerations. The interfaces of the fluid and the structure meshes are non-matching, so, the load and mesh motion are transferred by a conservative algorithm (principle of virtual work) [7].

2.2.3. Dynamic mesh solver

To update the positions of the fluid mesh nodes after the deformation of the structure, we resolve a discrete pseudo-structural system in the form

$$\tilde{K}X = K_c u, \tag{4}$$

where X is the vector of fluid mesh vertices displacements and u is the vector of structure displacements. $\tilde{K}$ is a fictitious stiffness matrix associated with the fluid mesh which is represented by a network of springs. Lineal springs are associated with mesh edges and torsional springs with each couple of edges (Figure 1). K_c is a transfer matrix describing the action of the motion of the structure.

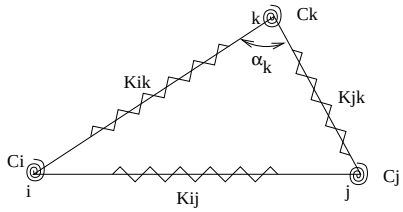

Figure 1: Springs network associated with the fluid mesh.

2.3. Temporal schemes

The fluid solver uses the fully implicit Gear's scheme which is second order accurate with three time levels. The derived non-linear equations are solved by a defect-correction method. The structure deformation is solved using the Newmark's scheme which is also implicit and second-order accurate.

2.3.1. The Geometric Conservation Law (GCL)

When integrating the semi-discretized equations between times t^n and t^{n+1}, we need to choose where to evaluate the integral of the different terms of equation (1) (ex: convective flux $\int_{t^n}^{t^{n+1}} F_i(w,x,\dot{x})\,dt$), i.e., on which mesh configuration we do integrate: at $(x^n,\dot{x}^n)$?, $(x^{n+1},\dot{x}^{n+1})$? or elsewhere? The Geometric Conservation Law states that the scheme must give an exact prediction of a uniform flow on a moving mesh while preserving consistency and stability. It was established [8] that the GCL is satisfied if the previous evaluation is done on four mesh configurations $(x^{n_k},\dot{x}^{n_k})$:

$$\int_{t^n}^{t^{n+1}} F_i(w,x,\dot{x})\,dt \simeq \Delta t^n \sum_{k=1}^{4} \omega_k F_i(w,x^{n_k},\dot{x}^{n_k}), \tag{5}$$

where ω_k is a suitable weight, $x^{n_k} = f(x^{n-1},x^n,x^{n+1})$ and $\dot{x}^{n_k} = g(\frac{x^n-x^{n-1}}{\Delta t^{n-1}}, \frac{x^{n+1}-x^n}{\Delta t^n})$.

2.3.2. The staggered coupling algorithm

The fluid/structure computations are coupled in time by the staggered algorithm given in [8, 7]. This algorithm is second order accurate and it follows the following steps:

1. At t^n, structure sends displacements u^n and velocities $\dot{u}^n$ of the F/S interface to the fluid.

2a. At $t^{n+\frac{1}{2}}$, the dynamic fluid mesh is updated with the boundary conditions $X^{n+\frac{1}{2}} = u^n + \frac{\Delta t}{2}\,\dot{u}^n$.

2b. The fluid state $W^{n+\frac{1}{2}}$ is computed on the updated mesh.

3. At $t^{n+\frac{1}{2}}$, fluid sends the pressure $P^{n+\frac{1}{2}}$ to the structure at F/S interface.

4. Finally, the displacements of the structure u^{n+1} are computed.

	thickness $[m]$	$E\,[MPa]$	ν	$\rho\,[kgm^{-3}]$
Extremities	0.02	70	0.33	2700
Hull	0.03	0.0041	0.5	1000

Table 1: Characteristics of the material of the structure.

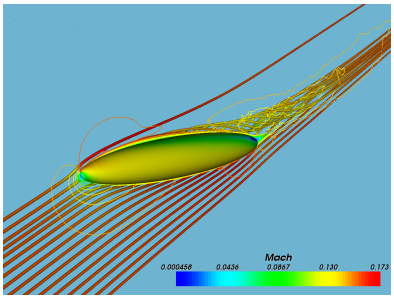

Figure 2: Time averaged streamlines around the spheroid

§3. Airship aeroelastic simulation

3.1. Studied configuration

The studied airship is represented by a $6:1$ prolate spheroid of $L = 1.37\,m$ length. The air flow Mach number at the free stream is $M_\infty = 0.15$. This flow is fully turbulent and is characterized by a Reynolds number of $Re_L = 4 \times 10^4$. Pressure and density at free stream are respectively $P_\infty = 1.013 \times 10^5\,Pa$ and $\rho_\infty = 1.1\,kg/m^3$. The airship fly is considered at lateral wind conditions, so the angle of attack is of $20°$.

The hull of the structure is flexible and pressurized. It is mainly made of rubber except at the extremities which are harder and made of metal. The table 1 gives the main characteristics of the used materials. The pressure inside the hull is fixed at $P_{in} = 1.1P_\infty$. The structure is fixed at its tail.

The unstructured fluid mesh used in this study is composed of 10^6 tetrahedra and 16×10^4 nodes. This mesh was decomposed in 32 non-overlapping subdomains. The structure mesh is a surface mesh containing 2274 nodes and 4544 triangular shell elements.

3.2. Results

The fluid flow computations are unsteady. It is also the case of structure computations, excepts that some suitable damping was added to the structure solver by using the Rayleigh's coefficients as in [9]. This way, the structure movement is made non-oscillatory and the final state is easily reached.

In the aim of future comparisons, we assume the same turbulence conditions of the flow as in [1] and [2], so the turbulence is activated at the position $x = 0.2L$ of the spheroid. Before this point, the flow is assumed non turbulent. Figure 2 shows the form of streamlines obtained for such a flow.

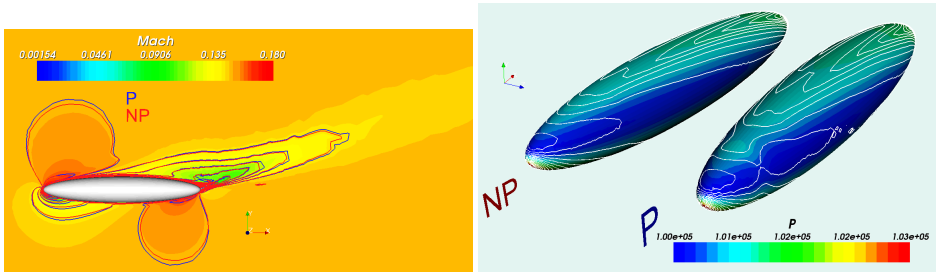

Figure 3: Time averaged Mach number isolines around pressurized and non-pressurized prolate (left) and pressure isolines on the hull surface

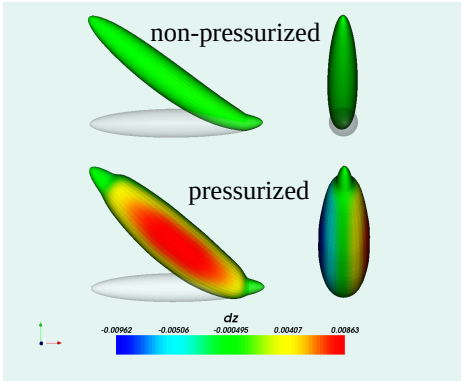

Figure 4: Final deformations of the structure ($\times 10$)

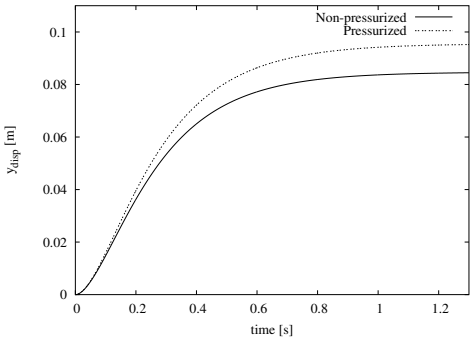

Figure 5: Evolution of the vertical displacement of the nose

In order to observe the influence of the pressurization on the strengthening of the structure, computations were made for both pressurized and non-pressurized structures. Figure 3 gives the Mach number distribution around the prolate for the two cases. We observe that they are quite similar. On the other hand, pressure distribution on the prolate surface is influenced by the pressurization as shown by the right graphics of the same figure. This is due to the resulting inflation of the flexible part of the hull.

The final form of the structure is given on the Figure 4, where the deformations are amplified 10 times for better visibility. The two structures are subject to comparable vertical bending, but the pressurized one is also substantially inflated. Quantitatively, the nose of the latest has a more important vertical displacement (Figure 5). We were expecting that pressurization will stiffen the prolate and make it less deformable. Actually, the enlargement of the prolate surface due to the inflation increases the aerodynamic forces applied to it. So, it is difficult in these conditions to distinguish the role of the inflation on the strengthening.

§4. Conclusion

In this study we have implemented a whole strategy to simulate the coupled behavior of a turbulent air flow and a pressurized deformable structure in order to appreciate the role of pressurization. This strategy combines a mesh mechanical system, and a fluid-structure pseudo-unsteady coupling method. The resulting algorithm is robust and could be accurately applied to the problem with one million tetrahedra. Convergence to steady fluid-structure coupling is obtained in a monotone and rather fast way. In the continuation of this work, more care must be taken in the choice of the dimensions, because, we noticed that for such a problem, the initial dimensions of the structure must be scaled so that, after inflation, it has the same surface area as the non-pressurized one, so that the two structures will be subject to the same aerodynamic forces and the comparison will make sense.
For such a flexible structure, we have encountered some particular difficulties for updating the dynamic mesh. This difficulties stem from the fact that the deformations are substantial while the fluid turbulent mesh is rather fine. The mesh solver needs a large amount of iterations to converge compared to the case involving metallic structure [3].

Acknowledgements

The authors are grateful to *Conseil Régional d'Aquitaine* for its financial support and thank the *Centre Informatique National de l'Enseignement Supérieur* (CINES) for providing the computational resources.

References

[1] CHESNAKAS, C. J., AND SIMPSON, R. L. A detailed investigation of the 3-*D* separation about a 6:1 prolate spheroid at angle of attack. *AIAA Journal 35*, 6 (1997), 990–999.

[2] CONSTANTINESCU, G. S., PASINATO, H., WANG, Y. Q., FORSYTHE, J. R., AND SQUIRES, K. D. Numerical investigation on flow past a prolate spheroid. *J. Fluids Eng. 124* (2002), 904–910.

[3] EL OMARI, K., SCHALL, E., KOOBUS, B., AND DERVIEUX, A. Inviscid flow calculation around a flexible airship. In *Actes des VIII Journées Zaragoza-Pau*. Monografías del Seminario Matemático García de Galdeano n. 31. Prensas Universitarias de Zaragoza, 2004, pp. 543–551.

[4] KOOBUS, B., FARHAT, C., AND TRAN, H. Computation of unsteady viscous flows around moving bodies using the $k--\varepsilon$ turbulent model on unstructured dynamic grids. *Comput. Methods Appl. Mech. Engrg. 190* (2000), 1441–1466.

[5] CAMARRI, S., SALVETTI, M. V., KOOBUS, B., AND DERVIEUX, A. Large-eddy simulation of a bluff-body flow on unstructured grids. *International Journal for Numerical Methods in Fluids 40* (2002), 1431–1460.

[6] EL OMARI, K., SCHALL, E., LE GUER, Y., AND AMARA, M. Numerical study of turbulent flow around a generic airship at high angle of attack. *4th International Conference on Computational Heat and Mass Transfer*, Paris (France), May 17-20, 2005, pp. 1361–1363.

[7] FARHAT, C., LESOINNE, M., AND LE TALLEC, P. Load and motion transfer algorithms for fluid/structure interaction problems with non-matching discrete interfaces: Momentum and energy conservation, optimal discretization and application to Aeroelasticity. *Computer Methods in Applied Mechanics and Engineering 157*, (1998), 95–114.

[8] KOOBUS, B., AND FARHAT, C. Second-order time-accurate and geometrically conservative implicit schemes for flow computations on unstructured dynamic meshes. *Computer Methods in Applied Mechanics and Engineering 170* (1999), 103–130.

[9] LARDAT, R., KOOBUS, B., RUFFINO, F., FARHAT, C. AND DERVIEUX, A.. Premières investigations du couplage fluide-structure autour d'un lanceur spatial générique. *INRIA Report*, N^o 4314, (2001).

K. El Omari, E. Schall, J-P. Dumas
and M. Amara
Université de Pau, LaTEP/LMA,
1 Av. de l'université 64000 Pau, France

B. Koobus
Université de Montpellier II
Place Eugène Bataillon, dépt. Math.
CC 051, F-34095 Montpellier Cedex 5
koobus@darboux.math.univ-montp2.fr

A. Dervieux
INRIA, 2003 Route des Lucioles
F-06902 Sophia-Antiplolis Cedex
alain.dervieux@inria.fr